Joint Transmit-and-Receive Antenna Selection System for MIMO-NOMA With Energy Harvesting

Mahmoud Aldababsa and Ertugrul Basar, *Senior Member, IEEE*

***Abstract*—In this article, outage probability (OP) of a joint transmit-and-receive antenna selection (JTRAS) scheme is analyzed in multiple-input–multiple-output nonorthogonal multiple-access-based downlink energy harvesting (EH) relaying networks. In this dual-hop and amplify-and-forward relaying-based network, since the first and second hops are types of single-user and multiuser systems, respectively, the optimal JTRAS and suboptimal majority-based JTRAS schemes are employed in the first and second hops. The theoretical OP analysis is carried out over Nakagami-*m* fading channels in the cases of perfect and imperfect successive interference cancellation. An asymptotic OP expression is also obtained at a high signal-to-noise ratio regime. Finally, Monte Carlo simulations are performed to substantiate the accuracy of the theoretical analysis. It is shown that the optimal power splitting ratios at the EH relay are different for users and the users with good channel conditions have minimum optimal ratios.**

***Index Terms*—Energy harvesting (EH), joint transmit-and-receive antenna selection (JTRAS), multiple-input–multiple-output (MIMO), nonorthogonal multiple access (NOMA), successive interference cancellation (SIC).**

I. Introduction

NONORTHOGONAL multiple access (NOMA) is one of the promising multiple-access candidates for beyond 5G wireless networks [1]. It has potential advantages in terms of spectral efficiency and massive connectivity. The distinctive feature of NOMA, especially power-domain NOMA, is that it serves multiple users simultaneously by allocating the same nonorthogonal resources and different power levels utilizing the superposition coding (SC) scheme at the transmitter, while uses the successive interference cancellation (SIC) principle to separate the superimposed signal at the receivers [2].

Most early works on NOMA focused on single-antenna NOMA networks [3], [4]. In particular, Yue *et al.* [3] present a unified framework of NOMA networks and assume imperfect SIC (ipSIC). In [4], the sum rate is maximized for a downlink NOMA system in the presence of ipSIC. Since multiantenna and cooperative communication systems can provide substantial performance benefits [5], the NOMA incorporates them, and thus, it attains better outage probability (OP) and ergodic rate compared to the conventional orthogonal multiple access [6]–[13]. Specifically, in [6], the OP performance of the NOMA-based relaying network is investigated over Rayleigh fading channels. In this network, a multiantenna base station (BS) communicates with multiantenna users through a channel state information (CSI)-based gain amplify-and-forward (AF) single-antenna relay. Also, the transmit antenna selection (TAS) and maximal ratio combining (MRC) schemes are applied at the BS and users, respectively. Then, the work [6] is extended to [7] and [8] for the CSI-based gain AF relay with imperfect CSI (ipCSI) [7], and for both CSI-based and fixed-gain AF relay in the ipCSI and ipSIC cases [8]. The OP performance of the maximum ratio transmission/receive antenna selection (MRT/RAS) technique is investigated with ipCSI in [9]. In [10], Toka *et al.* analyze the performance of the MRT/MRC scheme in a dual-hop NOMA full-duplex relay network in the presence of residual hardware impairments, ipCSI and ipSIC. The performance of space-time-block-code–aided cooperative NOMA is studied in [11] under ipSIC, ipCSI, and imperfect timing synchronization between distributed cooperating users. In [12], a downlink multiple-user multiple-input–multiple-output NOMA (MIMO-NOMA) relay system is investigated where all users are grouped into several clusters. Then, the exact closed-form expressions of the OP of each user in every cluster are derived for the cases of perfect SIC (pSIC) and ipSIC. So far, in [13], the secrecy OP performance of a multiple-relay-assisted NOMA network is examined over Nakagami-*m* fading channels.

It is noteworthy to mention that the previous wireless cooperative networks [6]–[13] do not take into account that the relay may have limited battery reserves and may need to rely on some external charging mechanism in order to remain active in the network. As a result, to cope with this practical problem, energy harvesting (EH) in such networks appears as a particularly important solution as it can enable information relaying. In this context, the study of the cooperative NOMA with wireless EH is carried out in [14]–[30]. Particularly, in [14], the achievable data rate is calculated for a two-user NOMA network such that the near user works as an EH relay for the far user. In [15], the ergodic sum-rate performance for the NOMA network with an AF EH relay is studied, and then, its upper bound expression is obtained. The OP expression is derived in closed form under Nakagami-*m* fading channels for the NOMA network with an AF EH relay [16]. The impact of the cochannel interferences and hardware impairments on the EH NOMA networks are examined in [17] and [18]–[20], respectively. In [21], the system performance of the cooperative

Manuscript received 6 February 2021; revised 18 May 2021 and 27 July 2021; accepted 28 August 2021. Date of publication 16 September 2021; date of current version 26 August 2022. This work was supported by the Scientific and Technological Research Council of Turkey (TUBITAK) under Grant 218E035. *(Corresponding author: Mahmoud Aldababsa.)*

The authors are with the Communications Research and Innovation Laboratory (CoreLab), Department of Electrical and Electronics Engineering, Koc University, 34450 Istanbul, Turkey (e-mail: m.dababsa87@gmail.com, ebasar@ku.edu.tr).

Digital Object Identifier 10.1109/JSYST.2021.3109306

EH-assisted cognitive radio NOMA is examined in terms of OP and throughput with ipSIC. The EH NOMA networks' performance is investigated through diverse relay selection techniques in [22]–[27]. Extended to the work [6], the OP performance is examined in [28] and [29] for EH AF and decode-and-forward relays, respectively. In [30], the OP performance is examined over Rayleigh fading channels for the NOMA-based EH relaying network, where the schemes joint transmit receive antenna selection (JTRAS) and RAS are employed in the first and second hops, respectively.

It is worth to mention that the authors in [15]–[29] use a relay with a single transmit and a receive antenna, while the authors in [30] use a relay with a single transmit and multiple receive antennas. However, relaying with multitransmit/receive antennas can offer a better system performance than that of relaying with a single antenna. Unfortunately, in the multiantenna systems, the hardware complexity and power requirements are higher compared to the single-antenna systems because each antenna requires an individual radio frequency (RF) chain for radio signal processing. Nevertheless, in order to exploit the advantages of the multiple antennas in all network nodes without extra power consumption and hardware complexity, antenna selection is expected to be employed in both hops. One of the well-known antenna selection schemes is optimal JTRAS (JTRAS-opt).[1] The JTRAS-opt scheme basically selects a transmit–receive antenna pair between two communication nodes and may be realized in the single-user communication network (as in the first hop). However, the JTRAS-opt scheme is not possibly realized in the multiuser NOMA networks (as in the second hop). This is because, in NOMA networks, all users have to be taken into account in order to find the best transmit–receive antenna pair, which may not be possible for all channel realizations to all users. As well, due to severe interuser interference, mathematical analyses of antenna-selection-based NOMA networks will be more difficult because of using SC and SIC methods at the transmitter and receiver, respectively. To solve this problem, the authors in [31] suggested a new suboptimal JTRAS scheme called majority-based JTRAS (JTRAS-maj). It basically selects the transmit–receive antenna pair with the majority. There are also another suboptimal antenna selection solutions such as max–max–max and max–min–max [32]–[34]. The max–max–max and max–min–max schemes are merely interested in optimizing the performance of strong and weak users, respectively, at the price of worse performance for the remaining users. On the other hand, the JTRAS-maj scheme yields a better performance for more than half users in NOMA networks, and the results in [31] prove the superiority of the JTRAS-maj scheme over the max–max–max- and max–min–max-based JTRAS schemes. Because of that, in this article, we attend to use the JTRAS-opt and JTRAS-maj schemes in the first and second hops, respectively.

[1]Although other antenna selection schemes such as TAS/MRC scheme may provide better performance than JTRAS, these schemes require multiple RF chains. However, with only one RF chain and simple circuitry, the JTRAS scheme can exploit the advantages of multiple antennas as well as decrease the complexity and power consumption. For these reasons, we consider the JTRAS scheme in this article.

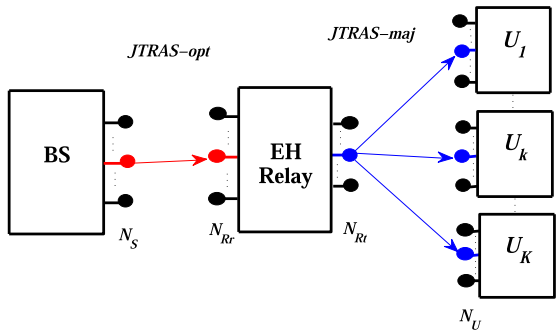

Fig. 1. Network model of the EH MIMO-NOMA network.

To the best of our knowledge, there have been few attempts to apply antenna-selection-based MIMO-NOMA into the EH relaying networks in the literature, which highly motivates this article. Furthermore, the SIC error (ipSIC) is also a practical and strong problem that NOMA networks encounter. The key contributions of this article can be highlighted as follows.

1) The OP performance is examined for cooperative MIMO-NOMA networks in both pSIC and ipSIC cases. In this network, the BS, EH relay, and users have multiple-antennas and the JTRAS-opt and JTRAS-maj schemes are applied in the first and second hops, respectively.
2) In the cases of pSIC and ipSIC, the exact OP expression is derived in closed form over the generic channel model independent identically distributed (i.i.d.) Nakagami-m fading, which also includes the special channel model line-of-sight when $m = 1$, i.e., Rayleigh fading.
3) The asymptotic analysis is carried out in order to demonstrate that the system achieves diversity order.
4) Finally, the theoretical results are validated by the Monte Carlo simulation. The results show that the optimum power division ratios by the power splitter at the EH relay are different for users and the users with good channel conditions will have less transmission power.

The numerical results also demonstrate that although ipSIC affects the OP performance, it does not affect the optimal power splitting ratios. Furthermore, the optimal EH relay location has to be closer to the BS and as the EH relay becomes near the users, the OP becomes worse and converges to the same value for all users. Moreover, the results show the superiority of the proposed JTRAS-maj scheme over the max–max–max and max–min–max-based JTRAS schemes.

The rest of this article is organized as follows. In Section II, the network model, antenna selection schemes, and signal-to-interference-and-noise ratio statistics are introduced. In Section III, the OP analysis is conducted. At last, numerical results are presented to verify the theoretical OP analysis in Section IV, and Section V concludes this article.

II. Network Model

In Fig. 1, we consider a cooperative MIMO-NOMA network in which a BS communicates with K users with the help of an AF EH relay. All nodes have multiple antennas such that

N_S transmit and N_U receive antennas are employed at the BS and each user, respectively, as well as N_{Rt} transmit and N_{Rr} receive antennas are equipped at the relay. We assume that the direct links between the BS and users are blocked. The channel coefficients corresponding to the BS relay and relay-U_k links are denoted by $\{h_{\text{SR}}^{(i,j)}, 1 \le i \le N_S, 1 \le j \le N_{Rr}\}$ and $\{h_{\text{RU}_k}^{(i,j)}, 1 \le i \le N_{Rt}, 1 \le j \le N_U\}$, respectively, where i and j refer, respectively, to the ith transmit and jth receive antennas corresponding to each communication node (BS, relay, and users).

The whole communication process between the BS and users is accomplished in two stages. At the first stage, the BS transmits $x_S = \sqrt{P_S a_k} s_k + \sum_{t \neq k}^{K} \sqrt{P_S a_t} s_t$ to the relay, where P_S, a_t, and s_t are the transmit power at the BS, power factor, and information of the user t, respectively. Based on NOMA, the power coefficients have two features; $a_1 + \cdots + a_K = 1$ and reversely ordered according to the second hop channel gains as $a_1 \ge \ldots \ge a_K$. If h_{SR} is the channel coefficient corresponding to the best link (the red link as shown in Fig. 1) from BS relay links, offering the highest channel gain between the BS and the relay, and n_R is zero mean complex additive Gaussian noise with a variance of σ_R^2 at the relay, then the received signal at the relay can be stated as

$$y_R = h_{\text{SR}} \sqrt{P_S a_k} s_k + h_{\text{SR}} \sum_{t \neq k}^{K} \sqrt{P_S a_t} s_t + n_R. \tag{1}$$

At the second stage, the relay harvests the energy from the signals transmitted by the BS following the power-splitting-based relaying protocol [35], and then, forwards the remaining information to the users. Note that the time τT is used to harvest energy from the BS, while the remaining time $(1-\tau)T$ is to deliver information to the users, where T is the total time frame, and $0 < \tau < 1$ is the fraction of the time frame used to harvest energy. In addition, it is worth notable that the relay does not use all the antennas to harvest the energy from the BS. This is because of applying the JTRAS scheme that utilizes only one RF chain between the BS and relay. The received signal y_R is split into two parts with $w : 1-w$ proportion by the power splitter. Specifically, $\sqrt{1-w} y_R$ is exploited as information to be processed, i.e., $\sqrt{1-w} y_R = \sqrt{1-w} h_{\text{SR}} \sqrt{P_S a_k} s_k + \sqrt{1-w} h_{\text{SR}} \sum_{t \neq k}^{K} \sqrt{P_S a_t} s_t + n_{\text{SR}}$, where $n_{\text{SR}} = \sqrt{1-w} n_R$ is the zero mean complex additive Gaussian noise with a variance of $\sigma_{\text{SR}}^2 = (1-w)\sigma_R^2$. The other part $\sqrt{w} y_R$ is harvested as the transmitting power at the relay in order to amplify the remaining $\sqrt{1-w} y_R$ signal with an amplification factor G and transmit it to K users. If the transmit power at the relay is

$$P_R = \zeta w P_S |h_{\text{SR}}|^2 \tag{2}$$

then the amplification factor can be expressed as

$$\begin{aligned} G &= \sqrt{\frac{P_R}{(1-w)P_S|h_{\text{SR}}|^2 + \sigma_{\text{SR}}^2}} \\ &= \sqrt{\frac{\zeta w P_S |h_{\text{SR}}|^2}{(1-w)P_S|h_{\text{SR}}|^2 + \sigma_{\text{SR}}^2}} \\ &\approx^{(a)} \sqrt{\frac{\zeta w P_S |h_{\text{SR}}|^2}{(1-w)P_S|h_{\text{SR}}|^2}} \\ &= \sqrt{\frac{\zeta w}{(1-w)}} \end{aligned} \tag{3}$$

where the step (a) is obtained by neglecting the value of σ_{SR}^2 as it is very small, $0 \le \zeta \le 1$ is the energy conversion efficiency, and $|\cdot|$ represents the absolute value operator. Accordingly, the received signal at the user k can be expressed as

$$\begin{aligned} y_{U_k} = & \underbrace{h_{\text{RU}_k} G \sqrt{1-w} h_{\text{SR}} \sum_{t=1}^{k-1} \sqrt{P_S a_t} s_t}_{\text{ipSIC term}} \\ & + \underbrace{h_{\text{RU}_k} G \sqrt{1-w} h_{\text{SR}} \sqrt{P_S a_k} s_k}_{\text{Desired signal term}} \\ & + \underbrace{h_{\text{RU}_k} G \sqrt{1-w} h_{\text{SR}} \sum_{t=k+1}^{K} \sqrt{P_S a_t} s_t}_{\text{Interference term}} \\ & + \underbrace{h_{\text{RU}_k} G n_{\text{SR}} + n_{U_k}}_{\text{Noise term}} \end{aligned} \tag{4}$$

where h_{U_k} is the channel coefficient corresponding to relay-users links between the majority transmit antenna at the relay and the best receive antennas at the users (the blue links as shown in Fig. 1),[2] n_{U_k} is the zero mean complex additive Gaussian noise with a variance of $\sigma_{U_k}^2$ at the user k. Note that the SIC is applied at the receiver to lessen the interference and yield reliable detection for the signals of the users. In particular, the receiver of the kth user cancels the interfered signals from $U_1, \ldots, U_{k-1}$ and treats $U_{k+1}, \ldots, U_K$ as interference. However, since SIC process is not being carried out perfectly, the term $\sum_{t=1}^{k-1} \sqrt{P_S a_t} s_t$ results in a propagation error modeled as a complex Gaussian random variable, i.e., $\sum_{t=1}^{k-1} \sqrt{P_S a_t} s_t$ is the zero mean complex Gaussian noise with a variance of $\xi \sum_{t=1}^{k-1} a_t P_S$, where $0 \le \xi \le 1$ is the error propagation factor [36]. It is worth mentioning that the received signal at the user k in the case of the pSIC can be simply expressed by putting $\xi = 0$ into (4).

A. Antenna Selection Schemes

As shown in Fig. 1, the JTRAS-opt [37] and suboptimal JTRAS-maj [31] schemes are applied in the first and second hops, respectively.

1) First Hop: In the first hop, the JTRAS-opt scheme chooses the transmit–receive antenna pair between the BS and the relay, (i_S, j_R), where $i_S \in \{1, \ldots, N_S\}$ is the selected transmit antenna at the BS and $j_R \in \{1, \ldots, N_{Rr}\}$ is the selected receive antenna at the relay. Precisely, (i_S, j_R) has the highest channel gain between the transmit antennas of BS and receiver antennas

[2]Recall, based on the NOMA concept, the power coefficients are ordered reversely to the second hop channel gains, i.e., $a_1 \ge \ldots \ge a_K$ opposite to $|h_{U_1}|^2 \le \ldots \le |h_{U_K}|^2$

of the relay and it can be determined as

$$(i_S, j_R) = \underset{\substack{1\le i\le N_S\\ 1\le j\le N_{Rr}}}{\arg\max} \left\{ |h_{\text{SR}}^{(i,j)}|^2 \right\}. \tag{5}$$

2) Second Hop: In the second hop, the JTRAS-maj scheme can be realized by first applying a JTRAS-opt [37] separately for the users. Therefore, the transmit–receive antenna pair, $(i_{\text{RU}_k}, j_{U_k})$, providing the highest channel gain between the BS and user k is determined, where $i_{\text{RU}_k} \in \{1, \ldots, N_{Rt}\}$ and $j_{U_k} \in \{1, \ldots, N_U\}$. Then, by the majority algorithm [31], the majority transmit antenna at the relay $i_R \in \{1, \ldots, N_{Rt}\}$ is specified. Accordingly, the $(i_{\text{RU}_k}, j_{U_k})$ and i_R can be determined, respectively, as

$$(i_{\text{RU}_k}, j_{U_k}) = \underset{\substack{1\le i\le N_{Rt}\\ 1\le j\le N_U}}{\arg\max} \left\{ |h_{\text{RU}_k}^{(i,j)}|^2 \right\}, k = 1, \ldots, K \tag{6}$$

$$i_R = \text{Maj}(i_{\text{RU}_k}) \tag{7}$$

where $\text{Maj}(\cdot)$ denotes the majority function that determines the majority transmit antenna through an algorithm given in detail in [31]. Briefly, the majority algorithm includes the following two steps. The first step is finding a set that consists of the best-selected antenna for each user. This step is carried out according to the well-known antenna selection criterion (JTRAS-opt). The second step is applying the majority rule to the set, which is determined in the first step. Accordingly, the best-selected antenna with the majority, which is available for more than half of users, will be selected.

B. Signal-to-Interference-and-Noise Ratio Statistics

From (4), the expression of the instantaneous signal-to-interference-and-noise ratio (SINR) of the U_k to detect the U_l can be derived in the case of ipSIC as

$$\gamma_{l,k} = \frac{\overline{\gamma}|h_{\text{SR}}|^2|h_{\text{RU}_k}|^2 a_l}{\overline{\gamma}|h_{\text{SR}}|^2|h_{\text{RU}_k}|^2\Sigma_l + c_1|h_{\text{RU}_k}|^2 + c_2}, l \neq K, l < k \tag{8}$$

where $\overline{\gamma} = \frac{P_S}{\sigma^2}$ is the SNR, $\sigma^2 = \sigma_{\text{SR}}^2 = \sigma_{U_k}^2$, $\Sigma_l = \xi \sum_{t=1}^{l-1} a_t + \sum_{t=l+1}^{K} a_t$, $c_1 = \frac{1}{1-w}$, and $c_2 = \frac{1}{\zeta w}$.

In this article, we assume that the magnitudes of the fading gains are i.i.d. with Nakagami-*m* distribution. Thus, the cumulative distribution function (CDF) and the probability density function (PDF) of the square of the Nakagami-*m* random variable X are stated, respectively, as

$$F_X(x) = \frac{\psi(m, \frac{m}{\Omega}x)}{\Gamma(m)} \tag{9}$$

$$f_X(x) = \left(\frac{m}{\Omega}\right)^m \frac{x^{m-1}}{\Gamma(m)} e^{-\frac{mx}{\Omega}} \tag{10}$$

where $\psi(\cdot,\cdot)$ and $\Gamma(\cdot)$ are lower incomplete Gamma and Gamma functions, respectively, m is the parameter of Nakagami-*m* distribution, and $\Omega = E[|X|^2]$, where $E[\cdot]$ refers to the expectation operator. Now, according to the selection criterion in (5), the CDF of the squared channel gain corresponding to the best link in the first hop is

$$F_{|h_{\text{SR}}|^2}(x) = (F_X(x))^{N_S N_{Rr}}. \tag{11}$$

Then, taking the derivative of (11), the PDF of the squared channel gain corresponding to the best link in the first hop is

$$f_{|h_{\text{SR}}|^2}(x) = N_S N_{Rr} f_X(x) (F_X(x))^{N_S N_{Rr}-1}. \tag{12}$$

Using (9) and (10) and exploiting the properties of $\psi(\cdot,\cdot)$ in [38], the $F_{|h_{\text{SR}}|^2}(x)$ and $f_{|h_{\text{SR}}|^2}(x)$ in (11) and (12), respectively, can be explicitly rewritten as

$$\begin{aligned} F_{|h_{\text{SR}}|^2}(x) &= \left(1 - e^{-\frac{m_{\text{SR}}}{\Omega_{\text{SR}}}x} \sum_{v=0}^{m_{\text{SR}}-1} \left(\frac{m_{\text{SR}}}{\Omega_{\text{SR}}}x\right)^v \frac{1}{v!}\right)^{N_S N_{Rr}} \\ &= \sum_{u=0}^{N_S N_{Rr}} \sum_{v=0}^{u(m_{\text{SR}}-1)} \binom{N_S N_{Rr}}{u} (-1)^u \\ &\quad \times \vartheta_v(u, m_{\text{SR}}) x^v e^{-\frac{u m_{\text{SR}}}{\Omega_{\text{SR}}}x} \end{aligned} \tag{13}$$

$$\begin{aligned} f_{|h_{\text{SR}}|^2}(x) &= N_S N_{Rr} \left(\frac{m_{\text{SR}}}{\Omega_{\text{SR}}}\right)^{m_{\text{SR}}} \frac{x^{m_{\text{SR}}-1}}{\Gamma(m_{\text{SR}})} e^{-\frac{m_{\text{SR}}}{\Omega_{\text{SR}}}x} \\ &\quad \times \left(1 - e^{-\frac{m_{\text{SR}}}{\Omega_{\text{SR}}}x} \sum_{n=0}^{m_{\text{SR}}-1} \left(\frac{m_{\text{SR}}}{\Omega_{\text{SR}}}x\right)^n \frac{1}{n!}\right)^{N_S N_{Rr}-1} \\ &= N_S N_{Rr} \left(\frac{m_{\text{SR}}}{\Omega_{\text{SR}}}\right)^{m_{\text{SR}}} \frac{x^{m_{\text{SR}}-1}}{\Gamma(m_{\text{SR}})} e^{-\frac{m_{\text{SR}}}{\Omega_{\text{SR}}}x} \\ &\quad \times \sum_{u=0}^{N_S N_{Rr}-1} \sum_{v=0}^{u(m_{\text{SR}}-1)} \binom{N_S N_{Rr}-1}{u} (-1)^u \\ &\quad \times \vartheta_v(u, m_{\text{SR}}) x^v e^{-\frac{u m_{\text{SR}}}{\Omega_{\text{SR}}}x} \end{aligned} \tag{14}$$

Note that in (13) and (14), $\vartheta_x(y, g_z)$ denotes multinomial coefficients, which can be defined as $\vartheta_x(y, g_z) = \frac{1}{x d_0} \sum_{i=1}^{x} (i(y+1) - x) d_i \vartheta_{x-y}(y, g_z)$, $x \geq 1$ [38, eq. (0.314)]. Here, $d_i = (g_z/\Omega_z)^i/i!$, $\vartheta_0(y, g_z) = 1$, and $\vartheta_x(y, g_z) = 0$ if $i > g_z - 1$.

On the other hand, according to the selection criteria in (6) and (7), the CDF of the squared channel gain corresponding to relay-U_k link between the majority transmit antenna at the relay and the best receive antenna at the user k, i.e., $F_{|h_{\text{RU}_k}|^2}(x)$ is given generally for K users as in (15), shown at the bottom of the next page [31, eq. (15)] (*see the proof in [31]*). In (15), $F_\varphi(x) = \left(\frac{\psi(m_{\text{RU}}, \frac{m_{\text{RU}}}{\Omega_{\text{RU}}}x)}{\Gamma(m_{\text{RU}})}\right)^{N_U}$, $\kappa_s = P_r(\varpi = s) = \frac{\binom{K}{\varpi}}{\sum_{j=0}^{\frac{K-1}{2}} \binom{K}{j}}$, $Q_{k,s} = \frac{(K-s)!}{(K-k)!(k-s-1)!}$, and $\zeta_s = \frac{(\frac{K-1}{2})!}{(\frac{K-1}{2}-s)!(s-1)!}$. For a special case, the CDF of the $F_{|h_{\text{RU}_k}|^2}(x)$ for $N_{Rt} = 2$ and $K = 3$ is given as [31, eq. (14)]

$$\begin{aligned} F_{|h_{\text{RU}_k}|^2}(x) &= \sum_{q=1}^{3N_{Rt}} \eta_{(k,q)} \\ &\quad \times \left(1 - e^{-\frac{m_{\text{RU}}}{\Omega_{\text{RU}}}x} \sum_{s=0}^{m_{\text{RU}}-1} \left(\frac{m_{\text{RU}}}{\Omega_{\text{RU}}}x\right)^s \frac{1}{s!}\right)^{qN_U} \end{aligned}$$

$$= \sum_{q=1}^{3N_{Rt}} \sum_{p=0}^{qN_U} \sum_{s=0}^{p(m_{\mathrm{RU}}-1)} \binom{qN_U}{p} (-1)^p \eta_{(k,q)} \times \vartheta_s(p, m_{\mathrm{RU}}) x^s e^{-\frac{pm_{\mathrm{RU}}}{\Omega_{\mathrm{RU}}}x} \quad (16)$$

where $\eta_{(1,1)} = \eta_{(1,2)} = \frac{3}{2}, \eta_{(1,3)} = -\frac{9}{2}, \eta_{(1,4)} = \frac{15}{4}, \eta_{(1,5)} = -\frac{3}{2}, \eta_{(1,6)} = \frac{1}{4}, \eta_{(2,3)} = 3, \eta_{(2,4)} = -\frac{3}{4}, \eta_{(2,5)} = -\frac{9}{4}, \eta_{(2,6)} = 1, \eta_{(3,5)} = \frac{3}{2}, \eta_{(3,6)} = -\frac{1}{2}$, and otherwise equal zero.

III. OP Analysis

A. Exact OP

The OP is defined as the probability that instantaneous SINR is below a threshold value. Now, define $\{\gamma_{l,k} < \gamma_{\mathrm{th}_l}\}, l = 1, \ldots, k$, as an event that the kth user cannot detect the lth user's message correctly, and $\{\gamma_{l,k} > \gamma_{\mathrm{th}_l}\}$ as the complementary event of $\{\gamma_{l,k} < \gamma_{\mathrm{th}_l}\}$. The OP of the kth user can be expressed as $\mathrm{OP}_k = 1 - P_r(\{\gamma_{1,k} > \gamma_{\mathrm{th}_1}\} \cap \ldots \cap \{\gamma_{k,k} > \gamma_{\mathrm{th}_k}\})$. Accordingly, by using (8) and under the condition $a_l - \Sigma_l \gamma_{\mathrm{th}_l} > 0$, the $\{\gamma_{l,k} > \gamma_{\mathrm{th}_l}\}$ can be stated as

$$\{\gamma_{l,k} > \gamma_{\mathrm{th}_l}\} = \left\{ |h_{\mathrm{RU}_k}|^2 > \frac{\frac{\gamma_{\mathrm{th}_l} c_1}{\overline{\gamma}(a_l - \Sigma_l \gamma_{\mathrm{th}_l})} c_2}{c_1 \left(|h_{\mathrm{SR}}|^2 - \frac{\gamma_{\mathrm{th}_l} c_1}{\overline{\gamma}(a_l - \Sigma_l \gamma_{\mathrm{th}_l})} \right)} \right\}. \quad (17)$$

Now, assume $\tau_k^* = \max\{\frac{\gamma_{\mathrm{th}_l} c_1}{\overline{\gamma}(a_l - \Sigma_l \gamma_{\mathrm{th}_l})}\}_{l=1,\ldots,k}$, then the OP_k can be written as

$$\begin{aligned}
\mathrm{OP}_k &= 1 - P_r\left(|h_{\mathrm{RU}_k}|^2 > \frac{\tau_k^* c_2}{c_1 (|h_{\mathrm{SR}}|^2 - \tau_k^*)}, |h_{\mathrm{SR}}|^2 > \tau_k^* \right) \\
&= 1 - \int_{\tau_k^*}^{\infty} \left(1 - F_{|h_{\mathrm{RU}_k}|^2}\left(\frac{\tau_k^* c_2}{c_1 (x - \tau_k^*)} \right) \right) f_{|h_{\mathrm{SR}}|^2}(x) dx \\
&= 1 - \int_{\tau_k^*}^{\infty} f_{|h_{\mathrm{SR}}|^2}(x) dx \\
&\quad + \int_{\tau_k^*}^{\infty} F_{|h_{\mathrm{RU}_k}|^2}\left(\frac{\tau_k^* c_2}{c_1 (x - \tau_k^*)} \right) f_{|h_{\mathrm{SR}}|^2}(x) dx \\
&= F_{|h_{\mathrm{SR}}|^2}(\tau_k^*) \\
&\quad + \underbrace{\int_{\tau_k^*}^{\infty} F_{|h_{\mathrm{RU}_k}|^2}\left(\frac{\tau_k^* c_2}{c_1 (x - \tau_k^*)} \right) f_{|h_{\mathrm{SR}}|^2}(x) dx}_{I_1}. \quad (18)
\end{aligned}$$

Considering the complexity of $F_{|h_{\mathrm{RU}_k}|^2}(x)$ in (15) generally for K users, we attend to avoid majority function's complexity and find the closed-form OP expression for the special case $K = 3$. Nevertheless, the system performance in term of the OP for the general case K users will be demonstrated numerically in Section IV.

Now, using (13), (14), and (16) in (18), I_1 can be rewritten as in (19), shown at the bottom of the next page.

Now, by change of variables $y = x - \tau_k^*$, then I_2 in (19) can be expressed as

$$I_2 = \int_0^{\infty} \left(\frac{\tau_k^* c_2}{c_1 y} \right)^s e^{-\frac{pm_{\mathrm{RU}}}{\Omega_{\mathrm{RU}}} \frac{\tau_k^* c_2}{c_1 y}} \underbrace{(y + \tau_k^*)^{m_{\mathrm{SR}}-1+v}}_{J} \times e^{\left(-\frac{m_{\mathrm{SR}}}{\Omega_{\mathrm{SR}}} - \frac{um_{\mathrm{SR}}}{\Omega_{\mathrm{SR}}}\right)(y+\tau_k^*)} dy. \quad (20)$$

Next, by the help of series expansion, J in (20) can be stated as $J = \sum_{z=0}^{m_{\mathrm{SR}}-1+v} \binom{m_{\mathrm{SR}}-1+v}{z} (\tau_k^*)^{m_{\mathrm{SR}}-1+v-z} y^z$. Substituting J into (20), I_2 can be rewritten as

$$\begin{aligned}
I_2 &= \left(\frac{\tau_k^* c_2}{c_1} \right)^s \sum_{z=0}^{m_{\mathrm{SR}}-1+v} \binom{m_{\mathrm{SR}} - 1 + v}{z} (\tau_k^*)^{m_{\mathrm{SR}}-1+v-z} \\
&\quad \times e^{\left(-\frac{m_{\mathrm{SR}}}{\Omega_{\mathrm{SR}}} - \frac{um_{\mathrm{SR}}}{\Omega_{\mathrm{SR}}}\right)\tau_k^*} \\
&\quad \times \int_0^{\infty} y^{z-s} e^{-\frac{pm_{\mathrm{RU}}\tau_k^* c_2}{\Omega_{\mathrm{RU}} c_1} y^{-1}} e^{\left(-\frac{m_{\mathrm{SR}}}{\Omega_{\mathrm{SR}}} - \frac{um_{\mathrm{SR}}}{\Omega_{\mathrm{SR}}}\right) y} dy. \quad (21)
\end{aligned}$$

Here, the integral in (21) can be calculated as $2(\frac{b_1}{b_2})^{\frac{z-s+1}{2}} K_{z-s+1}(2\sqrt{b_1 b_2})$ [38, eq. (3.471.9)], where $b_1 = \frac{pm_{\mathrm{RU}}\tau_k^* c_2}{\Omega_{\mathrm{RU}} c_1}$, $b_2 = \frac{m_{\mathrm{SR}}}{\Omega_{\mathrm{SR}}} + \frac{um_{\mathrm{SR}}}{\Omega_{\mathrm{SR}}}$, and $K_\beta(\cdot)$ denotes the βth order of the modified Bessel function of the second kind. Finally, using I_2, I_1 and (13) in (18), the exact closed-form OP expression in the case of the ipSIC can be expressed as in (22), shown at the bottom of the next page. By putting $\xi = 0$ into

$$F_{|h_{\mathrm{RU}_k}|^2}(x) = \begin{cases}
\kappa_0 \left(\frac{K!}{(K-1)!} \sum_{t=0}^{K-1} \frac{(-1)^t}{1+t} \binom{K-1}{t} F_\varphi^{1+t}(x) \right)^2 + \sum_{s=1}^{\frac{K-1}{2}} \kappa_s \left(1 - (1 - F_\varphi(x))^{2s} \right), & k = 1 \\
\kappa_0 \left(Q_{k,0} \sum_{t=0}^{K-l} \frac{(-1)^t}{k+t} \binom{L-l}{t} F_\varphi^{l+t}(x) \right)^2 + \\
\sum_{s=1}^{k-1} \kappa_s \left(Q_{k,s} \sum_{t=0}^{K-k} \frac{(-1)^t}{k-s+t} \binom{K-k}{t} F_\varphi^{k-s+t}(x) \right)^2 \zeta_s \sum_{t=0}^{\frac{K-1}{2}-s} \frac{(-1)^t}{s+t} \binom{\frac{K-1}{2}-s}{t} F_\varphi^{s+t}(x) + \\
\sum_{s=k}^{\frac{K-1}{2}} \kappa_s \left(1 - \left(1 - \zeta_s \sum_{t=0}^{\frac{K-1}{2}-s} \frac{(-1)^t}{s+t} \binom{\frac{K-1}{2}-s}{t} F_\varphi^{s+t}(x) \right)^{2s} \right), & 1 < k \le \frac{K-1}{2} \\
\kappa_0 \left(Q_{k,0} \sum_{t=0}^{K-k} \frac{(-1)^t}{k+t} \binom{K-k}{t} F_\varphi^{k+t}(x) \right)^2 \\
+ \sum_{s=1}^{\frac{K-1}{2}} \kappa_s \left(Q_{k,s} \sum_{t=0}^{K-k} \frac{(-1)^t}{k-s+t} \binom{K-k}{t} F_\varphi^{k-s+t}(x) \right)^2 \zeta_s \sum_{t=0}^{\frac{K-1}{2}-s} \frac{(-1)^t}{s+t} \binom{\frac{K-1}{2}-s}{t} F_\varphi^{s+t}(x), & \frac{K-1}{2} < k < K \\
\kappa_0 F_\varphi^{2K}(x) + \sum_{s=1}^{\frac{K-1}{2}} \kappa_s \left(Q_{K,s} \frac{1}{(K-s+t)} F_\varphi^{K-s+t}(x) \right)^2 \left(1 - (1 - F_\varphi(x))^2 \right)^s, & k = K
\end{cases} \quad (15)$$

(22), the exact OP expression in the case of the pSIC can be achieved in closed form as well.

B. Asymptotic OP

As the OP expression in (22) does not give us any insight, we analyze the asymptotic behavior of the OP performance of the network. For this reason, we use the high SNR approximation technique proposed in [39] and $\psi(x, y \to 0) \approx y^x/x$ [40, eq. (45.9.1)], then

$$F^{\infty}_{|h_{\text{SR}}|^2}(x) = \frac{\left(\frac{m_{\text{SR}}}{\Omega_{\text{SR}}}x\right)^{\mu_{\text{SR}}}}{\Gamma(m_{\text{SR}}+1)^{N_S N_{Rr}}} = \frac{\left(\frac{m_{\text{SR}}}{\Omega_{\text{SR}}}\right)^{\mu_{\text{SR}}}}{\Gamma(m_{\text{SR}}+1)^{N_S N_{Rr}}} x^{\mu_{\text{SR}}} \tag{23}$$

$$\begin{aligned} F^{\infty}_{|h_{\text{RU}_k}|^2}(x) &= \sum_{q=1}^{3N_{Rt}} \eta_{(k,q)} \frac{\left(\frac{m_{\text{RU}}}{\Omega_{\text{RU}}}x\right)^{\mu_{\text{RU}}}}{\Gamma(m_{\text{RU}}+1)^{qN_U}} \\ &= \sum_{q=1}^{3N_{Rt}} \eta_{(k,q)} \frac{\left(\frac{m_{\text{RU}}}{\Omega_{\text{RU}}}\right)^{\mu_{\text{RU}}}}{\Gamma(m_{\text{RU}}+1)^{qN_U}} x^{\mu_{\text{RU}}} \end{aligned} \tag{24}$$

where $\mu_{\text{SR}} = m_{\text{SR}} N_S N_{Rr}$ and $\mu_{\text{RU}} = q m_{\text{RU}} N_U$. Now, (19) can be rewritten as

$$\begin{aligned} \text{OP}_k &= P_r\left(\frac{|h_{\text{SR}}|^2 |h_{\text{RU}_k}|^2}{|h_{\text{RU}_k}|^2 + \nu} < \tau_k^*\right) \\ &= \underbrace{P_r\left(|h_{\text{SR}}|^2 < \tau_k^*\right)}(F_{|h_{\text{SR}}|^2}\tau_k^*) \\ &\quad + \underbrace{P_r\left(\tau_k^* < |h_{\text{SR}}|^2 < \frac{\nu\tau_k^*}{|h_{\text{RU}_k}|^2}\right)}_{\lambda} \end{aligned} \tag{25}$$

where $\nu = \frac{c_2}{c_1}$. From (25), the OP_k at the high SNR values can be calculated as $\text{OP}_k^{\infty} = F^{\infty}_{|h_{\text{SR}}|^2}(\tau_k^*) + \lambda^{\infty}$. $F^{\infty}_{|h_{\text{SR}}|^2}(\tau_k^*)$ can be found from (23) and λ^{∞} can be found as follows: first, λ can be written as

$$\begin{aligned} \lambda &= \int_{\tau_k^*}^{\infty} f_{|h_{\text{SR}}|^2}(x) \int_0^{\frac{\nu\tau_k^*}{x}} f_{|h_{\text{RU}_k}|^2}(y) dy dx \\ &= \int_{\tau_k^*}^{\infty} f_{|h_{\text{SR}}|^2}(x) F_{|h_{\text{RU}_k}|^2}\left(\frac{\nu\tau_k^*}{x}\right) dx. \end{aligned} \tag{26}$$

$f_{|h_{\text{SR}}|^2}(x)$ in (26) can roughly be stated as

$$f_{|h_{\text{SR}}|^2}(x) \approx \frac{\mu_{\text{SR}}\left(\frac{m_{\text{SR}}}{\Omega_{\text{SR}}}\right)^{\mu_{\text{SR}}-1}}{\Gamma(m_{\text{SR}}+1)^{N_S N_{Rr}}} x^{\mu_{\text{SR}}-1} e^{-\frac{m_{\text{SR}}}{\Omega_{\text{SR}}}x}. \tag{27}$$

By substituting (24) and (27) into (26), λ^{∞} can be expressed as

$$\begin{aligned} \lambda^{\infty} \approx{}& \frac{\mu_{\text{SR}}\left(\frac{m_{\text{SR}}}{\Omega_{\text{SR}}}\right)^{\mu_{\text{SR}}-1}}{\Gamma(m_{\text{SR}}+1)^{N_S N_{Rr}}} \\ &\times \sum_{q=1}^{3N_{Rt}} \eta_{(k,q)} \frac{\left(\frac{m_{\text{RU}}}{\Omega_{\text{RU}}}\right)^{\mu_{\text{RU}}} \nu^{\mu_{\text{RU}}} e^{-\frac{m_{\text{SR}}}{\Omega_{\text{SR}}}\tau_k^*}}{\Gamma(m_{\text{RU}}+1)^{qN_U} (\tau_k^*)^{-\mu_{\text{SR}}+1}} \\ &\times \underbrace{\int_0^{\infty} \frac{e^{-\frac{m_{\text{SR}}}{\Omega_{\text{SR}}}y}}{\left(\frac{y}{\tau_k^*}+1\right)^{\mu_{\text{RU}}-\mu_{\text{SR}}+1}} dy}_{I_4} \end{aligned} \tag{28}$$

$$\begin{aligned} I_1 &= \sum_{q=1}^{3N_{Rt}} \eta_{(k,q)} \left(1 - F_{|h_{\text{SR}}|^2}(\tau_k^*)\right) + \int_{\tau_k^*}^{\infty} F_{|h_{\text{RU}_k}|^2}\left(\frac{\tau_k^* c_2}{c_1(x-\tau_k^*)}\right) f_{|h_{\text{SR}}|^2}(x) dx \\ &= \sum_{q=1}^{3N_{Rt}} \eta_{(k,q)} \left(1 - F_{|h_{\text{SR}}|^2}(\tau_k^*)\right) + \sum_{q=1}^{3N_{Rt}} \sum_{p=1}^{qN_U} \sum_{s=0}^{p(m_{\text{RU}}-1)} \sum_{u=0}^{N_S N_{Rr}-1} \sum_{v=0}^{u(m_{\text{SR}}-1)} \binom{qN_U}{p} \binom{N_S N_{Rr}-1}{u} (-1)^{p+u} \eta_{(k,q)} \vartheta_s(p, m_{\text{RU}}) \\ &\quad \times \vartheta_v(u, m_{\text{SR}}) \frac{N_S N_{Rr}}{\Gamma(m_{\text{SR}})} \left(\frac{m_{\text{SR}}}{\Omega_{\text{SR}}}\right)^{m_{\text{SR}}} \underbrace{\int_{\tau_k^*}^{\infty} \left(\frac{\tau_k^* c_2}{c_1(x-\tau_k^*)}\right)^s e^{-\frac{p m_{\text{RU}}}{\Omega_{\text{RU}}} \frac{\tau_k^* c_2}{c_1\left(x-\tau_k^*\right)}} x^{m_{\text{SR}}-1+v} e^{\left(-\frac{m_{\text{SR}}}{\Omega_{\text{SR}}} - \frac{u m_{\text{SR}}}{\Omega_{\text{SR}}}\right)x} dx}_{I_2} \end{aligned} \tag{19}$$

$$\begin{aligned} \text{OP}_k &= \sum_{q=1}^{3N_{Rt}} \eta_{(k,q)} + \left(1 - \sum_{q=1}^{3N_{Rt}} \eta_{(k,q)}\right) \sum_{u=0}^{N_S N_{Rr}} \sum_{v=0}^{u(m_{\text{SR}}-1)} \binom{N_S N_{Rr}}{u} (-1)^u \vartheta_v(u, m_{\text{SR}}) (\tau_k^*)^v e^{-\frac{u m_{\text{SR}}}{\Omega_{\text{SR}}}\tau_k^*} \\ &\quad + \sum_{q=1}^{3N_{Rt}} \sum_{p=1}^{qN_U} \sum_{s=0}^{p(m_{\text{RU}}-1)} \sum_{u=0}^{N_S N_{Rr}-1} \sum_{v=0}^{u(m_{\text{SR}}-1)} \sum_{z=0}^{m_{\text{SR}}-1+v} \binom{qN_U}{p} \binom{N_S N_{Rr}-1}{u} \binom{m_{\text{SR}}-1+v}{z} (-1)^{p+u} \eta_{(k,q)} \vartheta_s(p, m_{\text{RU}}) \\ &\quad \times \vartheta_v(u, m_{\text{SR}}) \frac{2N_S N_{Rr}}{\Gamma(m_{\text{SR}})} \left(\frac{m_{\text{SR}}}{\Omega_{\text{SR}}}\right)^{m_{\text{SR}}} \left(\frac{\tau_k^* c_2}{c_1}\right)^s (\tau_k^*)^{m_{\text{SR}}-1+v-z} e^{\left(-\frac{m_{\text{SR}}}{\Omega_{\text{SR}}} - \frac{u m_{\text{SR}}}{\Omega_{\text{SR}}}\right)\tau_k^*} \left(\frac{b_1}{b_2}\right)^{\frac{z-s+1}{2}} K_{z-s+1}(2\sqrt{b_1 b_2}) \end{aligned} \tag{22}$$

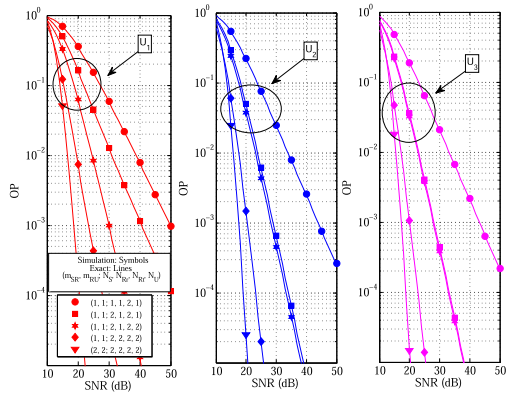

Fig. 2. OP versus SNR in the case of pSIC with different antenna configurations, channel conditions, $w = 0.5$, and $\zeta = 0.8$.

where I_4 can be approximated as [41, eq. (11)]

$$I_4 \approx \begin{cases} -\ln\left(\frac{m_{\text{SR}}}{\Omega_{\text{SR}}}\right)\tau_k^*, & \mu_{\text{SR}} = \mu_{\text{RU}} \\ \frac{\Gamma(-\mu_{\text{RU}}+\mu_{\text{SR}})}{\left(\frac{m_{\text{SR}}}{\Omega_{\text{SR}}}\right)^{-\mu_{\text{RU}}+\mu_{\text{SR}}}}(\tau_k^*)^{\mu_{\text{RU}}-\mu_{\text{SR}}+1}, & \mu_{\text{SR}} > \mu_{\text{RU}} \\ \frac{\Gamma(\mu_{\text{RU}}-\mu_{\text{SR}})}{\Gamma(\mu_{\text{RU}}-\mu_{\text{SR}}+1)}\tau_k^*, & \mu_{\text{SR}} < \mu_{\text{RU}} \end{cases}. \quad (29)$$

Next, if (23) and (28) are substituted into OP_k^∞, then OP_k^∞ can be obtained. As noticed that OP_k^∞ is proportional with τ_k^*, which means that at high SNR values, the system achieves diversity gain.

IV. Numerical Results

In this section, we present theoretical results verified by Monte Carlo simulations to demonstrate the accuracy of the EH MIMO-NOMA network's OP analysis. For this, in all theoretical and simulation results, unless otherwise stated, we assume $K = 3$, the users' power factors and their threshold SINR values are adjusted as $(a_1, \gamma_{\text{th}_1}) = (0.6, 1.4)$, $(a_2, \gamma_{\text{th}_2}) = (0.3, 2.2)$, $(a_3, \gamma_{\text{th}_3}) = (0.1, 2.5)$, $\Omega_{\text{SR}} = (d_{\text{SR}})^{-\alpha}$, and $\Omega_{\text{RU}} = (d_{\text{RU}})^{-\alpha}$, where d_{SR} and d_{RU} are the normalized distance between the BS and relay, the relay and users, respectively, and α is the path loss exponent. Here, $d_{\text{SR}} = 1 - d_{\text{RU}} = 0.5$ and $\alpha = 2$ unless otherwise stated.

Fig. 2 plots the OP versus SNR with different antenna configurations and channel conditions. Here, we assume that $w = 0.5$, $\zeta = 0.8$, and $\xi = 0$, i.e., a special case of pSIC. As expected, the analytical and simulation results match perfectly. Besides, the OP performance enhances as N_S and/or N_{Rr} and/or N_U increases and channel conditions $(m_{\text{SR}}, m_{\text{RU}})$ improve. In addition, OP_1 reduces considerably when the numbers of the antennas of the first and/or second hops (N_S, N_{Rr}, N_U) increase, while OP_2 and OP_3 improve when the number of the antennas of the first hop (N_S, N_{Rr}) increases rather than when the number of the receive antennas of the second hop (N_U) increases. For ease exposition, Tables I and II are given to provide, respectively, the values of the SNR that required to achieve $\text{OP} = 10^{-3}$ and the SNR gain advantage of different parameters of $(m_{\text{SR}}, m_{\text{RU}}; N_S, N_{Rr}, N_{Rt}, N_U)$ for each user. Precisely, under the condition of $(m_{\text{SR}}, m_{\text{RU}}) = (1, 1)$ to

TABLE I
Values of SNR (in dB) That Required to Achieve $\text{OP} = 10^{-3}$ for Each User With Different Parameters of $(m_{\text{SR}}, m_{\text{RU}}; N_S, N_{Rr}, N_{Rt}, N_U)$

$(m_{SR}, m_{RU}; N_S, N_{Rr}, N_{Rt}, N_U)$	U_1	U_2	U_3
$(1, 1; 1, 1, 2, 1)$	50	44.5	44
$(1, 1; 2, 1, 2, 1)$	41	29	28.5
$(1, 1; 2, 1, 2, 2)$	30	28.5	28.3
$(1, 1; 2, 2, 2, 2)$	23.5	21	20
$(2, 2; 2, 2, 2, 2)$	18.5	17.5	17

TABLE II
SNR Gain Advantage of Different Parameters of $(m_{\text{SR}}, m_{\text{RU}}; N_S, N_{Rr}, N_{Rt}, N_U)$ for Each User

SNR gain advantage of (in dB)	U_1	U_2	U_3
$(1, 1; 2, 1, 2, 1)$ over $(1, 1; 1, 1, 2, 1)$	9	15.5	15.5
$(1, 1; 2, 1, 2, 2)$ over $(1, 1; 2, 1, 2, 1)$	11	0.5	0.2
$(1, 1; 2, 2, 2, 2)$ over $(1, 1; 2, 1, 2, 2)$	6.5	7.5	8
$(2, 2; 2, 2, 2, 2)$ over $(1, 1; 2, 2, 2, 2)$	5	3.5	3

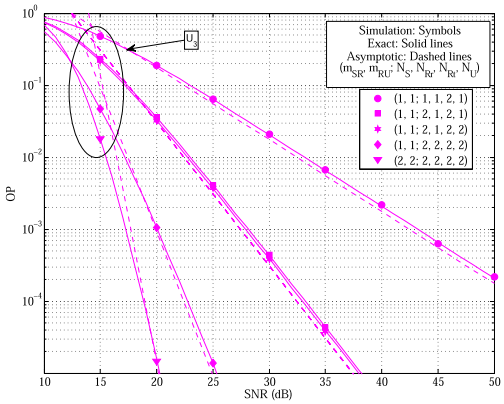

Fig. 3. OP_3 and asymptotic OP_3 versus SNR in the case of pSIC with different antenna configurations, channel conditions, $w = 0.5$, and $\zeta = 0.8$.

achieve $\text{OP}_1 = 10^{-3}$, 9-dB, 11-dB, and 6.5-dB SNR gain advantages are obtained for $(N_S, N_{\text{Rr}}, N_{\text{Rt}}, N_U) = (2, 1, 2, 1)$ over (1,1,2,1), (2,1,2,2) over (2,1,2,1), and (2,2,2,2) over (2,1,2,2), respectively. However, to achieve $\text{OP}_2 = \text{OP}_3 = 10^{-3}$, about 15.5-, 0.5-, and 8-dB SNR gain advantages are observed for (2,1,2,1) over (1,1,2,1), (2,1,2,2) over (2,1,2,1), and (2,2,2,2) over (2,1,2,2), respectively. On the other hand, under the condition of $(N_S, N_{Rr}, N_{Rt}, N_U) = (2, 2, 2, 2)$, to achieve $\text{OP}_1 = \text{OP}_3 = \text{OP}_3 = 10^{-3}$, we observe 5-, 3.5-, and 3-dB SNR gain advantages for $(m_{\text{SR}}, m_{\text{RU}}) = (2, 2)$ over (1,1), respectively. In order to see the behavior of the system performance in high SNR values, we demonstrate the OP_3 and its corresponding asymptotic versus SNR in Fig. 3. As seen, the asymptotic curves are compatible with the exact ones, and the diversity order of the network is obtained at high SNR values. Note that for the sake of the clarity, we only provide the OP and the corresponding asymptotic for the third user. However, this is also valid for the other users. Next, to demonstrate the effect of ipSIC on the OP performance, Fig. 4 shows the OP versus SNR with different values of ξ and antenna configurations $(N_S, N_{Rr}, N_{Rt}, N_U)$. Here, $(m_{\text{SR}}, m_{\text{RU}}) = (1, 1)$, $w = 0.5$, and $\zeta = 0.8$ are assumed. It is noticed that the OP_2 and OP_3 increase when ξ increases.

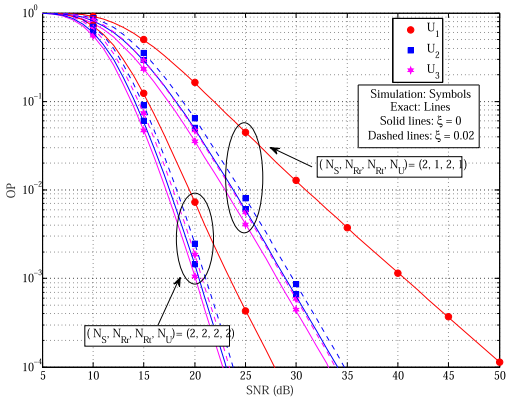

Fig. 4. OP versus SNR in the case of ipSIC with different values of ξ, antenna configurations $(N_S, N_{Rr}, N_{Rt}, N_U)$, $(m_{\text{SR}}, m_{\text{RU}}) = (1, 1)$, $w = 0.5$, and $\zeta = 0.8$.

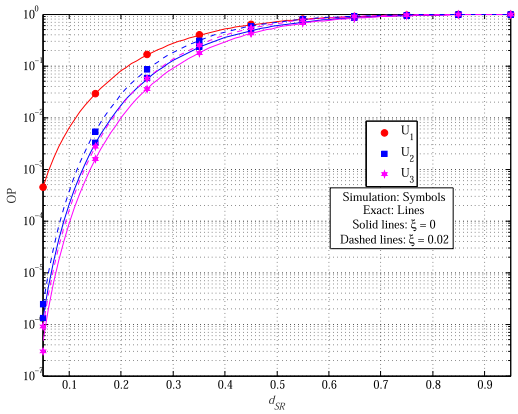

Fig. 6. OP versus d_{SR} with different values of ξ, $(m_{\text{SR}}, m_{\text{RU}}; N_S, N_{Rr}, N_{Rt}, N_U) = (1, 1; 2, 2, 2, 2)$, SNR $= 10$ dB, $w = 0.5$, and $\zeta = 0.8$.

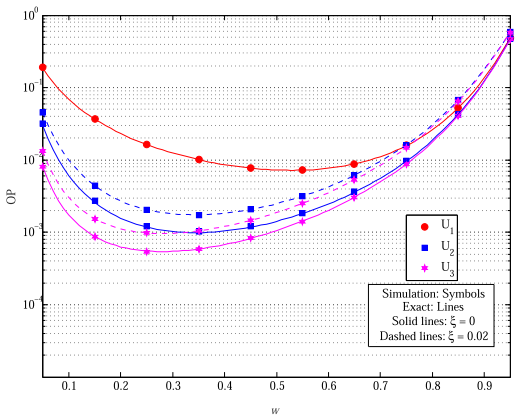

Fig. 5. OP versus w with different values of ξ, $(m_{\text{SR}}, m_{\text{RU}}; N_S, N_{Rr}, N_{Rt}, N_U) = (1, 1; 2, 2, 2, 2)$, SNR $= 20$ dB, and $\zeta = 0.8$.

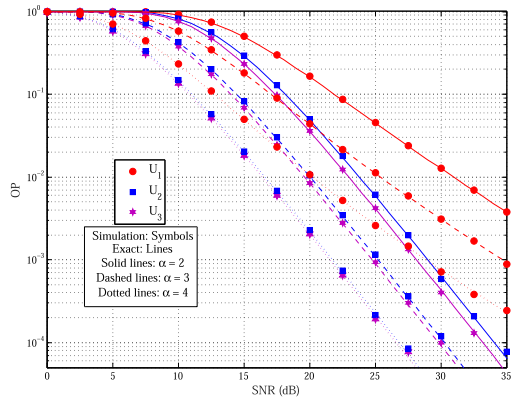

Fig. 7. OP versus SNR with different values of α, $(m_{\text{SR}}, m_{\text{RU}}; N_S, N_{Rr}, N_{Rt}, N_U) = (1, 1; 2, 1, 2, 1)$, $w = 0.5$, $\zeta = 0.8$, and $\xi = 0$.

In other words, the OP performance for U_2 and U_3 deteriorates in the case of ipSIC $(\xi = 0.02)$ rather that in the case of pSIC $(\xi = 0)$. However, OP_1 is not affected by ipSIC since U_1 does not require the SIC process to detect its signal.

Fig. 5 depicts the OP versus power division ratio w with different values of ξ. Here, $(m_{\text{SR}}, m_{\text{RU}}; N_S, N_{Rr}, N_{Rt}, N_U) = (1, 1; 2, 2, 2, 2)$, SNR $= 20$ dB, and $\zeta = 0.8$ are assumed. As clearly seen, in both pSIC and ipSIC, the optimum power division ratios for the three users are different from each other. The reason behind this phenomenon is that each user experiences different channel conditions and accordingly the user that has better channel conditions will have less transmission power. For instance, since the U_3 has a better channel condition than the other users, the transmission from the relay to the U_3 can be performed with less power than the others. Hence, U_3 takes a smaller value, which is about $w_3^{\text{opt}} = 0.25$. On the other hand, U_1 has the worst channel condition than the other users, the transmission from the relay to the U_1 can be done with high power than the others, which means that U_1 takes a higher value and from the graph, it is approximate $w_1^{\text{opt}} = 0.55$. Finally, U_2 is in between other users, and hence, it takes about $w_2^{\text{opt}} = 0.35$. It is notable to mention that the optimum power division ratios for the three users are not affected by ipSIC and this is maybe due to that the SIC process is done at the users and any error results only affect the OP, not the optimum power division rations at the EH relay. Fig. 6 presents the OP performance versus the normalized distance d_{SR} with different values of ξ. Here, $(m_{\text{SR}}, m_{\text{RU}}; N_S, N_{Rr}, N_{Rt}, N_U) = (1, 1; 2, 2, 2, 2)$, SNR $= 10$ dB, $w = 0.5$, and $\zeta = 0.8$ are assumed. It is obvious that in both pSIC and ipSIC, for all users, the OP performance becomes better when the EH relay is located near to the BS. On the other hand, the OP becomes worse, and finally, converges to the same value for all users when the EH relay is located far away BS (too much near to the users). One of the reasons for this is that the energy harvested in the relay decreases with the bad condition of the channel between the BS and the relay. Another reason is that the signal transmitted to the users declines due to the bad channel. As a result, the optimal relay location has to be closer to the BS. Fig. 7 depicts the OP versus SNR with different values of α. Here, we assume the parameters $(m_{\text{SR}}, m_{\text{RU}}; N_S, N_{Rr}, N_{Rt}, N_U) = (1, 1; 2, 1, 2, 1)$, $w = 0.5$, $\zeta = 0.8$, and $\xi = 0$. As clearly seen from Fig. 7, the OP performance enhances as the path loss exponent increases. In addition, we notice that the value of the OP is equal to unity till SNR of 10, 5, and 1 dB for $\alpha = 2, 3,$

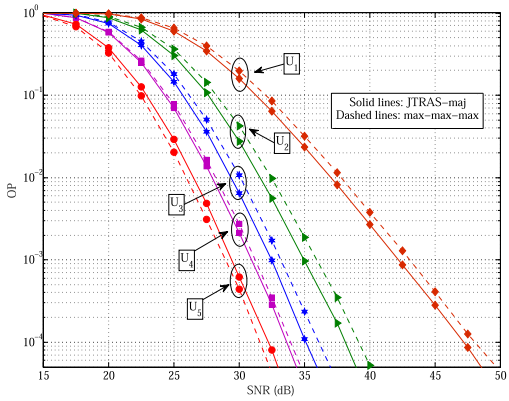

Fig. 8. Comparison between JTRAS-maj and max–max–max schemes for $K = 5$ users, $(m_{\text{SR}}, m_{\text{RU}}; N_S, N_{Rr}, N_{Rt}, N_U) = (1, 1; 2, 2, 2, 2)$, $w = 0.1$, $\zeta = 0.1$, and $\xi = 0$.

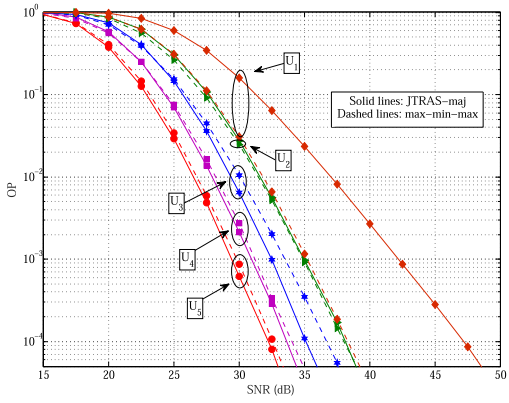

Fig. 9. Comparison between JTRAS-maj and max–min–max schemes for $K = 5$ users, $(m_{\text{SR}}, m_{\text{RU}}; N_S, N_{Rr}, N_{Rt}, N_U) = (1, 1; 2, 2, 2, 2)$, $w = 0.1$, $\zeta = 0.1$, and $\xi = 0$.

and 4, respectively. Figs. 8 and 9 demonstrate comparisons between the majority-based JTRAS, and max–max–max-based JTRAS and max–min–max-based JTRAS, respectively. For the comparison, we apply the JTRAS-opt scheme in the first hop and (JTRAS-maj or max–max–max or max–min–max) scheme in the second hop. Here, we assume that $K = 5$ users, the users' power factors and their threshold SINR values are adjusted as $(a_1, \gamma_{\text{th}_1}) = (0.45, 0.8)$, $(a_2, \gamma_{\text{th}_2}) = (0.25, 0.8)$, $(a_3, \gamma_{\text{th}_3}) = (0.15, 0.9)$, $(a_4, \gamma_{\text{th}_4}) = (0.1, 1.5)$, and $(a_5, \gamma_{\text{th}_5}) = (0.05, 2)$ as well as the parameters $(m_{\text{SR}}, m_{\text{RU}}; N_S, N_{Rr}, N_{Rt}, N_U) = (1, 1; 2, 2, 2, 2)$, $w = 0.1$, $\zeta = 0.1$, and $\xi = 0$. Recall that the max–max–max and max–min–max schemes are designed in order to maximize the performance of strong and weak users, respectively. On the other hand, the majority-based AS is designed to maximize the performance of more than half users. We clearly observe from both figures that the JTRAS-maj scheme has superiority over the max–max–max and max–min–max schemes. In particular, in Fig. 8, the JTRAS-maj scheme provides a better OP performance for four users (U_1, U_2, U_3, and U_4), while the max–max–max scheme offers better OP performance for only one user (U_5). On the other hand, in Fig. 9, the JTRAS-maj scheme offers a better OP performance for three users (U_3, U_4, U_5), while the max–min–max scheme offers a better OP performance for only one user (U_1). To sum up, we can notice from the results of this analysis that while designing practical communication systems, some considerations have to be taken into accounts. For instance, the antennas should be carefully employed since the OP performance of the users with bad channel conditions considerably improves as the number of antennas of both hops increases, while the OP performance of users with good channel conditions remarkably enhances when the number of the antennas of the first hop increases. In addition, the SIC error should be considered well as it affects the OP performance especially for the user that uses the SIC processes during decoding their signals. Also, the power division ratios have to specified carefully as each user has a different value from others. An EH relay should be located correctly in order to achieve a better OP performance. Moreover, the path loss has to be considered during the design since it influences the OP performance significantly.

V. Conclusion

In this article, the outage behavior of an EH MIMO-NOMA network with the JTRAS scheme has been examined in both pSIC and ipSIC cases. An OP analysis has been conducted over Nakagami-*m* fading channels and the exact OP expression is derived in closed form. The theoretical results have been verified by the Monte Carlo simulation. The results demonstrate that the OP performance enhances as the number of the antennas increases and channel conditions. Besides, the diversity order of the network is achieved at high SNR values. Moreover, the OP performance becomes worse in the case of ipSIC rather than that in the case of pSIC. Furthermore, the optimum power division proportions at the EH relay are different for users and the user with good channel conditions will have less transmission power. In addition, the optimal EH relay location has to be closer to the BS and as the EH relay becomes near the users, the OP becomes worse and converges to the same value for all users. The OP performance enhances as the path loss exponent increases. As well, the proposed JTRAS-maj scheme is superior to the max–max–max and max–min–max-based JTRAS schemes.

References

[1] Y. Liu *et al.*, " Nonorthogonal multiple access for 5G and beyond," *Proc. IEEE*, vol. 105, no. 12, pp. 2347–2381, Dec. 2017.
[2] S. M. R. Islam *et al.*, "Power-domain non-orthogonal multiple access (NOMA) in 5G systems: Potentials and challenges," *IEEE Commun. Surv. Tut.*, vol. 19, no. 2, pp. 721–742, Apr.–Jun. 2017.
[3] X. Yue *et al.*, "A unified framework for non-orthogonal multiple access," *IEEE Trans. Commun.*, vol. 66, no. 11, pp. 5346–5359, Nov. 2018.
[4] I. Abu Mahady, *et al.*, "Sum-rate maximization of NOMA systems under imperfect successive interference cancellation," *IEEE Commun. Lett.*, vol. 23, no. 3, pp. 474–477, Mar. 2019.
[5] B. Kumbhani and R. S. Kshetrimayum, "Source and relay transmit antenna selection in two hop cooperative communication systems over $k - \mu$ fading channels," in *Proc. 22nd Nat. Conf. Commun.*, 2016, pp. 1–5.
[6] J. Men and J. Ge, "Non-orthogonal multiple access for multiple-antenna relaying networks," *IEEE Commun. Lett.*, vol. 19, no. 10, pp. 1686–1689, Oct. 2015.
[7] Y. Zhang *et al.*, "Performance analysis of nonorthogonal multiple access for downlink networks with antenna selection over Nakagami-m fading channels," *IEEE Trans. Veh. Technol.*, vol. 66, no. 11, pp. 10590–10594, Nov. 2017.

[8] M. Aldababsa and O. Kucur, "Outage and ergodic sum-rate performance of cooperative MIMO-NOMA with imperfect CSI and SIC," *Int. J. Commun. Syst.*, vol. 33, no. 11, Jul. 2020, Art. no. e4405.
[9] M. Aldababsa and O. Kucur, "Performance of cooperative multiple-input multiple-output NOMA in Nakagami-m fading channels with channel estimation errors," *IET Commun.*, vol. 14, no. 2, pp. 274–281, Jan. 2020.
[10] M. Toka *et al.*, "Performance analyses of MRT/MRC in dual-hop NOMA full-duplex AF relay networks with residual hardware impairments," Feb. 2021. [Online]. Available: https://arxiv.org/abs/2102.08464v1
[11] M. W. Akhtar *et al.*, "STBC-aided cooperative NOMA with timing offsets, imperfect successive interference cancellation, and imperfect channel state information," *IEEE Trans. Veh. Technol.*, vol. 69, no. 10, pp. 11712–11727, Oct. 2020.
[12] T. M. Hoang *et al.*, "Outage analysis of MIMO-NOMA relay system with user clustering and beamforming under imperfect CSI in Nakagami-m fading channels," in *Proc. Conf. Ind. Netw. Intell. Syst.*, Aug. 2019, vol. 293, pp. 3–17.
[13] H. Lei *et al.*, "Secrecy outage analysis for cooperative NOMA systems with relay selection schemes," *IEEE Trans. Commun.*, vol. 67, no. 9, pp. 6282–6298, Sep. 2019.
[14] J. Li *et al.*, "Performance study of cooperative non-orthogonal multiple access with energy harvesting," in *Proc. 2nd Int. Conf. Commun. Eng. Technol.*, Nagoya, Japan, 2019, pp. 30–34.
[15] M. Hu *et al.*, "Ergodic sum rate analysis for non-orthogonal multiple access relaying networks with energy harvesting," in *Proc. 2nd IEEE Adv. Inf. Manag., Commun., Electron. Autom. Control Conf.*, Xi'an, China, 2018, pp. 474–477.
[16] N. Dahi and N. Hamdi, "Outage performance in cooperative NOMA systems with energy harvesting in Nakagami-m fading," in *Proc. 7th Int. Conf. Commun. Netw.*, Hammamet, Tunisia, 2018, pp. 1–4.
[17] P. Son and H. Kong, "Co-channel interference energy harvesting for decode-and-forward relaying," *Wireless Pers. Commun.*, vol. 95, no. 4, pp. 3629–3652, Aug. 2017.
[18] P. Son and H. Kong, "Energy-harvesting decode-and-forward relaying under hardware impairments," *Wireless Pers. Commun.*, vol. 96, no. 2, pp. 6381–6395, Jun. 2017.
[19] T. Le and H. Kong, "Performance analysis of downlink NOMA-EH relaying network in the presence of residual transmit RF hardware impairments," *Wireless Netw.*, vol. 26, no. 2, pp. 1045–1055, Feb. 2020.
[20] T. Le and H. Kong, "Effects of hardware impairment on the cooperative NOMA EH relaying network over Nakagami-m fading channels," *Wireless Pers. Commun.*, vol. 116, pp. 3577–3597, Nov. 2020.
[21] D. Do *et al.*, "NOMA in cooperative underlay cognitive radio networks under imperfect SIC," *IEEE Access*, vol. 8, pp. 86180–86195, 2020.
[22] P. Son *et al.*, "Exact outage analysis of a decode-and-forward cooperative communication network with *N*th-best energy harvesting relay selection," *Ann. Telecommun.*, vol. 71, no. 5, pp. 251–263, Jun. 2016.
[23] V. Tuan and H. Kong, "Impact of residual transmit RF impairments on energy harvesting relay selection systems," *Int. J. Electron.*, vol. 104, no. 6, pp. 928–941, Feb. 2017.
[24] W. Guo and W. Guo, "Non-orthogonal multiple access networks with energy harvesting and cooperative communication," in *Proc. 5th Int. Conf. Inf. Sci. Control Eng.*, Zhengzhou, China, 2018, pp. 1163–1167.
[25] L. Dung *et al.*, "Analysis of partial relay selection in NOMA systems with RF energy harvesting," in *Proc. 2nd Int. Conf. Adv. Signal Process., Telecommun. Comput.*, Ho Chi Minh City, Vietnam, 2018, pp. 13–18.
[26] S. Rao, "Relay selection for energy harvesting cooperative NOMA," *IEEE Int. Conf. Adv. Netw. Telecommun. Syst.*, Goa, India, 2019, pp. 1–6.
[27] A. Salem *et al.*, "Secrecy outage probability of energy-harvesting cooperative NOMA transmissions with relay selection," *IEEE Trans. Green Commun. Netw.*, vol. 4, no. 4, pp. 1130–1148, Dec. 2020.
[28] W. Han *et al.*, "Performance analysis for NOMA energy harvesting relaying networks with transmit antenna selection and maximal-ratio combining over Nakagami-m fading," *IET Commun.*, vol. 10, no. 18, pp. 2687–2693, 2016.
[29] Q. Wang *et al.*, "Performance analysis of NOMA for multiple-antenna relaying networks with energy harvesting over Nakagami-m fading channels," in *Proc. IEEE/CIC Int. Conf. Commun. China*, Qingdao, China, 2017, pp. 1–5.
[30] B. Demirkol and O. Kucur, "Outage performance of antenna selection schemes in NOMA networks using amplify-and-forward energy harvesting relay," in *Proc. 28th Signal Process Commun. Appl. Conf.*, Gaziantep, Turkey, 2020, pp. 1–4.
[31] M. Aldababsa and O. Kucur, "Majority based antenna selection schemes in downlink NOMA network with channel estimation errors and feedback delay," *IET Commun.*, vol. 14, no. 17, pp. 2931–2943, Oct. 2020.
[32] Y. Yu *et al.*, "Antenna selection for MIMO nonorthogonal multiple access systems," *IEEE Trans. Veh. Technol.*, vol. 67, no. 4, pp. 3158–3171, Apr. 2018.
[33] Q. Li *et al.*, "Joint antenna selection for MIMO-NOMA networks over Nakagami-m fading channels," in *Proc. IEEE/CIC Int. Conf. Commun. China*, Qingdao, China, 2017, pp. 1–6.
[34] Y. Yu *et al.*, "Antenna selection in MIMO cognitive radio-inspired NOMA systems," *IEEE Commun. Lett.*, vol. 21, no. 12, pp. 2658–2661, Dec. 2017.
[35] A. A. Nasir *et al.*, "Relaying protocols for wireless energy harvesting and information processing," *IEEE Trans. Wireless Commun.*, vol. 12, no. 7, pp. 3622–3636, Jul. 2013.
[36] A. Han, T. Lv, and X. Zhang, "Outage performance of NOMA-based UAV-Assisted communication with imperfect SIC," in *Proc. IEEE Wireless Commun. Netw. Conf.*, Marrakesh, Morocco, 2019, pp. 1–6.
[37] A. Yílmaz and O. Kucur, "Unified analysis of transmit, receive and hybrid diversity techniques over generalized-K channels," *Wireless Commun. Mobile Comput.*, vol. 16, no. 13, pp. 1798–1808, 2016.
[38] I. S. Gradshteyn and I. M. Ryzhik, *Table of Integrals, Series, and Products*, 7th ed. San Diego, CA, USA: Academic Press, 2007.
[39] Z. Wang and G. B. Giannakis, "A simple and general parameterization quantifying performance in fading channels," *IEEE Trans. Commun.*, vol. 51, no. 8, pp. 1389–1398, Aug. 2003.
[40] K. B. Oldham, J. Myland, and J. Spanier, *An Atlas of Functions With Equator, The Atlas Function Calculator*, 2nd ed. Berlin, Germany: Springer, 2008.
[41] F. Xu, F. Lau and D. Yue, "Diversity order for amplify-and-forward dual-hop systems with fixed-gain relay under Nakagami fading channels," *IEEE Trans. Wireless Commun.*, vol. 9, no. 1, pp. 92–98, Jan. 2010.

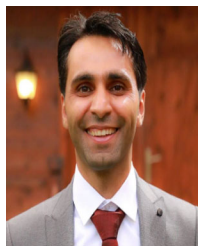

Mahmoud Aldababsa received the B.Sc. degree in electrical engineering from An-Najah National University, Nablus, Palestine, in 2010, the M.Sc. degree in electronics and communication engineering from Al-Quds University, Jerusalem, Palestine, in 2013, and the Ph.D. degree in electronics engineering from Gebze Technical University, Gebze, Turkey, in 2020.

He was a Research Assistant with Al-Quds University from 2010 to 2013. He is currently a Postdoctoral Researcher with Koç University, Istanbul, Turkey. His research interests include nonorthogonal multiple access and reconfigurable intelligent surface in future wireless generations.

Ertugrul Basar (Senior Member, IEEE) received the Ph.D. degree in electronics and communications engineering from Istanbul Technical University, Istanbul, Turkey, in 2013.

He is currently an Associate Professor with the Department of Electrical and Electronics Engineering, Koç University, Istanbul, Turkey, where he is also the Director of Communications Research and Innovation Laboratory (CoreLab). His research interests include beyond 5G systems, index modulation, intelligent surfaces, waveform design, and signal processing for communications. Dr. Basar is currently a Senior Editor for the IEEE COMMUNICATIONS LETTERS and an Editor for the IEEE TRANSACTIONS ON COMMUNICATIONS and *Frontiers in Communications and Networks*. He is a Young Member of Turkish Academy of Sciences.